Mon. Not. R. Astron. Soc. **000**, 000–000 (0000) Printed 10 January 2018 (MN LATEX style file v2.2)

How large are the Mg II haloes around young galaxies at $z \geqslant 5$?

Sarah E. I. Bosman[1], Alex Codoreanu[2]
[1] *Department of Physics and Astronomy, University College London, Gower Street, London WC1E 6BT, UK*
[2] *Centre for Astrophysics and Supercomputing, Swinburne University of Technology, Hawthorn, Victoria 3122, Australia*
[3] *ARC Centre of Excellence for All-sky Astrophysics (CAASTRO)*

ABSTRACT
We present a simple analytical model for constraining the sizes of Mg II regions around young galaxies at $5 \leqslant z < 7$. Using a compilation of recent high-redshift measurements, we find that enriched regions around bright ($M_{\rm AB} = -18$) galaxies must have sizes $R < 200$ ckpc to remain consistent with both the luminosity function of galaxies and occurrence rates of intervening absorbers towards background quasars. At the same time, we find that the lack of confirmed galaxy-absorber pairs in the fields around background quasars strongly implies a limiting magnitude of enrichment $M_{\rm min} > -19$. This result might help guide observational attempts to find such galaxy-absorber pairs. Finally, we produce a chart of smallest enriched region size versus choice of limiting magnitude for enrichment, which might be of use for numerical models of metal enrichment as a guide for required resolution.

1 INTRODUCTION

Metal enrichment in the circum- and meta-galactic medium is a leading probe of galaxy evolution. At low and intermediate redshifts, the composition of metal-enriched gas studied in the emission and absorption has yielded unique insight into the nature of galactic inflows and outflows. However, metal enrichment at high redshift currently poses both a theoretical and observational challenge.

There are a few reasons why the exploration of metal enrichment at $z > 5$ is increasingly complicated. First, the huge distances involved, coupled with lower metallicities at early times, mean that emission from excited ions is unresolved with current instruments unless lensing is involved. At the same time, the sparsity of bright background sources seriously limits the study of transverse detections of metal-enriched regions. Without the details of gaseous multi-phase processes which are visible in low-redshift galaxies, the trends observed in occurrence statistics of high-redshift metals remain sparse and puzzling.

On tracer of enrichment which has been studied consistently across redshift is the occurrence of the Mg II $\lambda\lambda$2796.3542 2803.5314Å doublet along quasar lines of sight. This feature is a widely used tracer of cool, ionised gas, associated with various properties of star-forming galaxies (e.g. Churchill et al. 1999, 2013; Ménard & Chelouche 2009; Weiner et al. 2009; Chen et al. 2010; Kacprzak et al. 2011; Matejek & Simcoe 2012). The transition has been used to probe the properties of low-luminosity galaxies, intra-cluster gas, and L_* galaxies (Churchill et al. 1999; Gauthier 2013; Bergeron & Boissé 1991; Steidel et al. 1994).

Paragraph on observational studies

Paragraph on numerical studies

In this letter, we aim to use a simple analytical model to convert lines-of-sight occurrence statistics of Mg II absorption into constraints on the sizes of Mg II -enriched haloes around galaxies (R) at $7 > z > 5$. We present the full range of $R(M_{AB})$ relations presently allowed by the observations. This formulation of current observations will be of use to numerical modellers wishing to resolve metal enrichment effects beyond $z = 5$, as well as observers looking for the elusive transverse metal enrichment at those redshifts.

Paragraph on structure of paper

2 ANALYTICAL MODEL

The following derivation, first outlined in Steidel (1995), offers a way to link the number density of absorbers (dN/dX or dN/dz) to the radius of enriched regions, given known relations for the luminosity function (LF, $\Phi(L)$) and a form of the R-luminosity relation. The number of absorbers per absorption path-length is given by

$$\frac{dN}{dX} = \frac{c\sigma n}{H_0} \tag{1}$$

where the 'gas cross-section' $n\sigma$ is given by

$$n\sigma = \pi \int_{L_{\rm min}}^{\infty} f_R(L)\Phi(L)R^2(L)dL, \tag{2}$$

and the pathlength X is defined as

$$\frac{dX}{dz} = (1+z)^2 \, \frac{H_0}{H(z)} \tag{3}$$

.

The luminosity function $\Phi(L)$ has empirically been determined to be well described by a Schechter function down

	dN/dX	source
$z = 5$	0.86 ± 0.19	Codoreanu et al. (2017)
$z = 6.5$	$1.00^{+0.75}_{-0.5}$	Bosman et al. (2017)

Table 1. Current measurements of occurrence rates of Mg II absorption. The measurements are sensitive to systems with $W_{\rm rest} \geqslant 0.1$Å. Value from Bosman et al. (2017) incorporates the data from Chen et al. (2016) over the same range.

β	f	$L_{\rm min}/L^*$
$[0.1 - 0.5]$	$[0.5 - 1.0]$	$[0.0001 - 1.0]$

Table 2. Allowed ranges for parameters which have not been directly measured at $z > 5$.

to magnitudes $M_{AB} \leqslant -15.0$:

$$\Phi(L)dL = \Phi^*(L/L^*)^{\alpha}\exp(-L/L^*)dL. \quad (4)$$

The LF is determined by two parameters Φ^*, α. At $5 < z < 7$, the determinations of these parameters by various authors are mildly discrepant, mostly due to systematic uncertainties (Bouwens et al. 2016). since our aim is to determine the range of enrichment radii permitted by observations, we include all current measurements of Φ^*, α in our error budget. The range of values used herein are displayed in Table 3.

The scaling of enrichment radius with galaxy luminosity has been successfully modelled at low redshift by a Holmberg-like power-law (Bergeron & Boissé 1991),

$$R(L) = R^*(L/L^*)^{\beta}. \quad (5)$$

This relation is remarkably tight at low redshift, for instance, Nielsen et al. (2013) find $\beta = 0.23 \pm 0.01$ for a population of 182 absorber-galaxy pairs at $0.072 \leqslant z \leqslant 1.120$. However, the size of ionised regions is set by the luminosities of host galaxies and the strength of the ultra-violet background (UVB), at least one of which is known to be changing rapidly at the end of hydrogen reionisation (e.g. Stark et al. 2010; Forero-Romero et al. 2012). It is therefore highly unclear how $R(L)$ should evolve with redshift, and we decide to use the full range of $\beta = [0.1, 0.5]$ with a flat prior to reflect the uncertainty. Throughout the paper we use a pivot $L^* = 9.61 \cdot 10^{36}$ erg s^{-1}, corresponding to to $M^*_{AB} = -21.2$.

Grouping expressions (5) and (4) into (2), we obtain,

$$\begin{aligned} n\sigma &= \pi \int_{L_{\rm min}}^{\infty} \Phi^* {R^*}^2 (L/L^*)^{\alpha+2\beta}\exp(-L/L^*)dL \\ &= \pi\Phi^* {R^*}^2 \Gamma(\alpha + 2\beta + 1, L_{\rm min}/L^*) \end{aligned} \quad (6)$$

Where Γ is the upper incomplete gamma function, and $L_{\rm min}$ is the limiting magnitude of enriched galaxies. Note that by construction, $L_{\rm min}$ is the magnitude of the faintest galaxies for which Mg II is detectable, i.e., $W_{\rm rest} \geqslant 0.1$Å.

Finally, using (1) we obtain,

$$\frac{dN}{dX} = f_R(L)\frac{c\pi}{H_0}\Phi^* {R^*}^2 \Gamma(\alpha + 2\beta + 1, L_{\rm min}/L^*), \quad (7)$$

or equivalently,

$$R^2 = \frac{H_0}{c\pi} f^{-1} \left(\frac{L}{L^*}\right)^{2\beta} \frac{dN}{dX} {\phi^*}^{-1} \Gamma^{-1}\left(\alpha + 2\beta + 1, L_{min}/L^*\right). \quad (8)$$

	α	ϕ^*	source
$z = 5$	-1.75 ± 0.13	$0.000758^{+0.00056}_{-0.00022}$	Mason et al. (2015)
	-1.76 ± 0.06	$0.00079^{+0.00023}_{-0.00018}$	Bouwens et al. (2015)
	$-1.67^{+0.05}_{-0.06}$	$0.000895^{+0.000192}_{-0.000131}$	Finkelstein et al. (2015)
$z = 6$	$-2.10^{+0.08}_{-0.03}$	0.00023 ± 0.00002	Livermore et al. (2017)
	$-2.02^{+0.10}_{-0.10}$	$0.000186^{+0.000094}_{-0.000080}$	Finkelstein et al. (2015)
$z = 7$	$-2.07^{+0.05}_{-0.04}$	0.00021 ± 0.00002	Livermore et al. (2017)
	$-2.04^{+0.17}_{-0.13}$	$0.00028^{+0.00051}_{-0.00018}$	Atek et al. (2015)
	$-1.94^{+0.09}_{-0.11}$	$0.00050^{+0.00013}_{-0.00018}$	Ishigaki et al. (2015)
	$-2.03^{+0.21}_{-0.20}$	$0.000157^{+0.000149}_{-0.000095}$	Finkelstein et al. (2015)

Table 3. Current measurements of the UV LF parameters α and Φ^* from various recent studies. The mild discrepancies are most likely due to systematic differences between measurement techniques.

Tables 1 and 2 show the most current constraints on α, Φ^* and dN/dX, which we will use in the next section. While measurements of α over $5 \leqslant z \leqslant 7$ are consistent among all published studies within error, this is not the case for the other luminosity function parameter Φ^*. Much debate is ongoing regarding this topic, with the leading proposed source of systematics being a mis-estimation of the lensing model uncertainties. We are not concerned in this paper with obtaining the most precise value of Φ^*, but simply exploring all models allowed within observational constraints. We therefore adopt the maximally conservative approach of an 'allowed range' for Φ^* extending from the one-sigma lowest allowed value by any author, to the highest one-sigma allowed value by any author in the recent literature. This yields bounds of $\Phi^* \in [0.0007, 0.001]$ at $z = 5.0$, $\Phi^* \in [0.0001, 0.00028]$ at $z = 6.0$, and $\Phi^* \in [0.000062, 0.00079]$ at $z = 7.0$.

Table 3 gives the allowed parameter ranges for β, f and $L_{\rm min}/L^*$, which have not been measured directly at these redshifts. Values of $\beta = 0.23 \pm 0.01$ and $f = 0.84 \pm 0.04$ have been measured by Nielsen et al. (2013) at $0.072 < z < 1.120$, but these values are expected to be different in the early universe as galaxy formation is ongoing, the UVB is patchier, and metal enrichment has not reached present-day levels. The value of $L_{\rm min}$, the limiting luminosity above which galaxies contain Mg II , is even more unconstrained and we accordingly treat it as a free parameter.

3 DISCUSSION

3.1 $R(L)$

The relation $R(L) = R^*(L/L^*)^{\beta}$ only depends on two parameters L_{min} and β, with R^* being obtainable from measured quantities using Equation (7). Figure 1 illustrates the effect of varying L_{min} and β while keeping all measured parameters fixed at their respective means, while Figure 2 shows the full range of all permitted models in varying parameters within their observational errors.

This enables us to put constraints on the maximal extent of Mg II enriched regions as a function of galaxy luminosity. For instance, the enriched regions around galaxies with $M_{AB} = -13$ cannot be larger 25 ckpc in any permissible model. Brighter galaxies with $M_{AB} \sim -18$ similarly

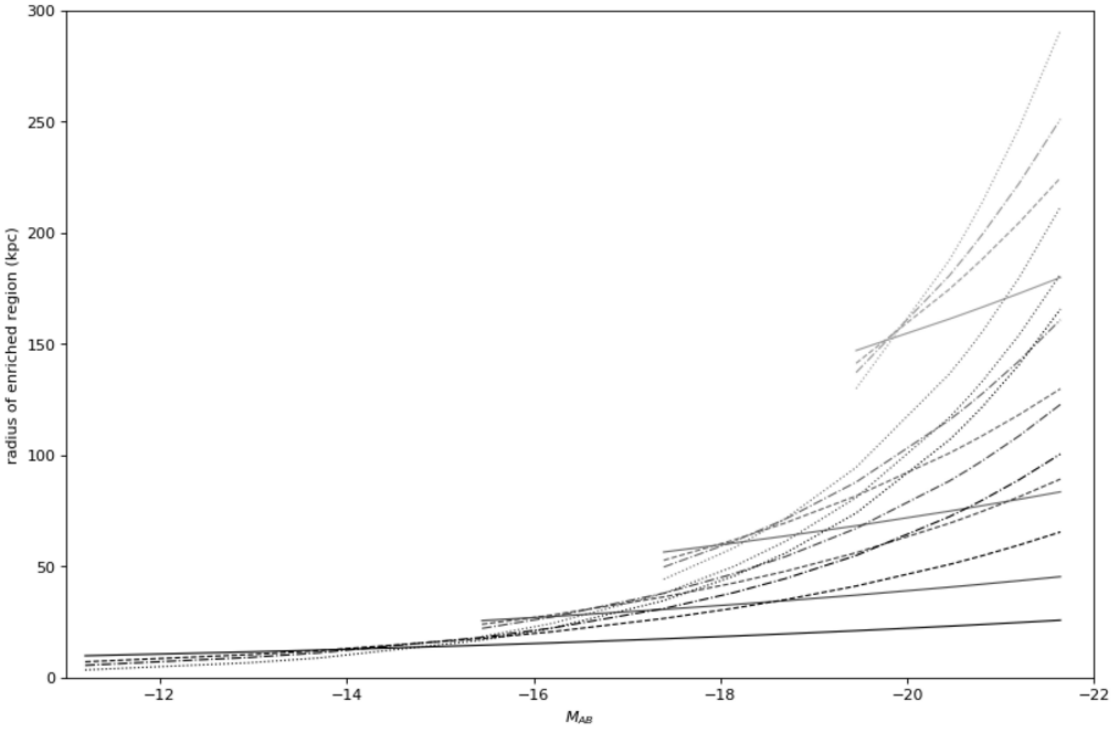

Figure 1. Relation between an object's AB magnitude and the expected size of the surrounding Mg II enriched region. Shades of grey correspond to varying $L_{\rm min}/L^* = 0.0001, 0.001, 0.01, 0.1$ corresponding to limiting magnitudes of $M_{\rm min} = -11.2, -13.7, -16.2, -18.7$, from dark to light. Line shape shows the effect of varying $\beta = 0.1, 0.23, 0.3, 0.4$, from continuous to dashed to dotted. Not all lines extend to low luminosities, since those systems are not enriched if $M_{\rm min}$ is high.

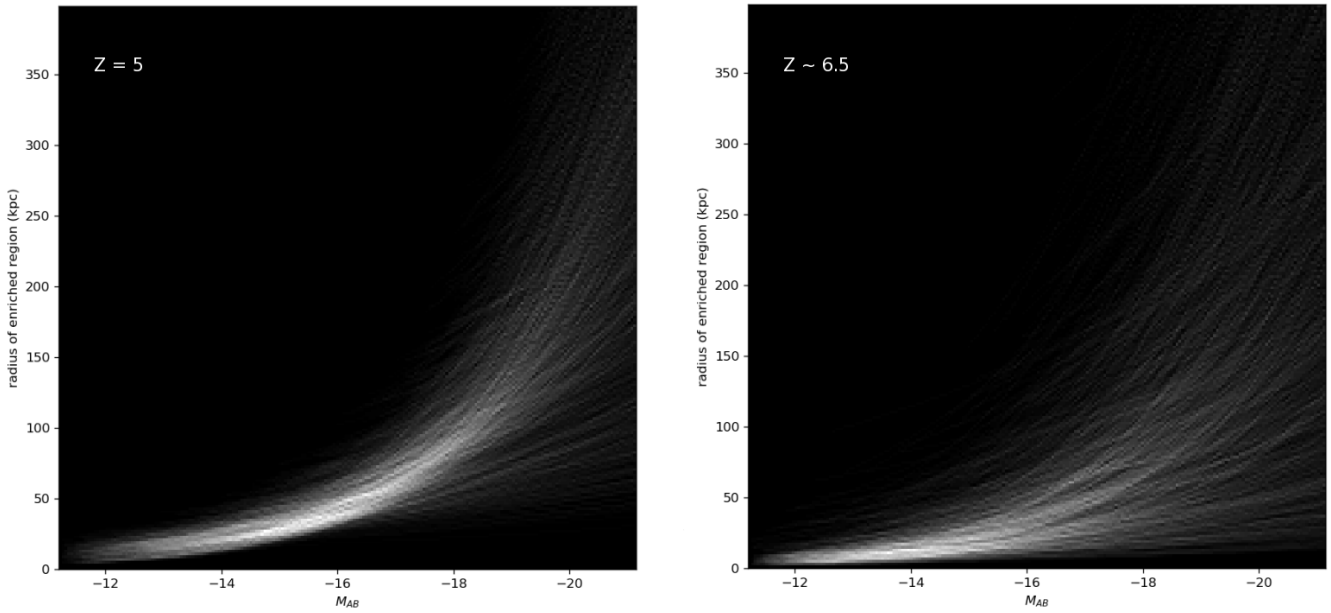

Figure 2. Same as Figure 1 for a continuum of models, with all parameters in equation (8) sampled from the allowed ranges given in Tables 1,2 and 3. The regions through which the largest number of models pass are shown in lighter grey, but depend strongly on the choice of prior used for sampling $L_{\rm min}$ (and to a lesser extend Φ^*). This figure showcases the full range of models which are compatible with observational constraints, as opposed to establishing which are more likely. However, some models can be excluded based on negative detections of galaxy-absorber pairs towards quasars as discussed in the text.

cannot possess Mg II regions larger than 200 ckpc, corresponding to 5.2" at $z = 5$. Indeed, enriched regions above these sizes would lead to higher dN/dX measurements towards high-redshift quasars, or would require fewer galaxies than predicted from measurements of the luminosity function $\Phi(L)$, or extremely low metal enrichment efficiencies ($f < 0.5$). The discovery of even a single such instance would put considerable strain on current models, or indicate the presence of a density correlation over large distances, such as a proto-cluster of galaxies.

Models with large values of $L_{\rm min}$, in which only the brightest galaxies produce enriched regions, might already be ruled out by the lack of confirmed galaxy-absorber pairs in observations of fields around quasars. Such models, shown in light gray in Figure 1, predict that galaxies corresponding to line-of-sight absorbers should be both bright and have large radii, and should therefore be readily visible in the surrounding fields. For instance, in models with $M_{\rm min} = -18.7$, enriched regions always possess radii $R > 140$ ckpc corresponding to 3.6" on the sky. Assuming random alignment, the probability of confusion of such a galaxy with the central quasar in an instrument such as MUSE is roughly $\lesssim 2\%$. A handful of non-detections therefore suffice to confidently constrain $M_{\rm min} > -19$.

In other words, if the galaxies corresponding to Mg II absorbers were distant from the quasar line-of-sight, they would be bright enough to be detectable in current exposures of surrounding fields. On the other hand, if the galaxies are sufficiently close to the line of sight to be confused with the central object, they would very likely have been inadvertently included in the slit spectroscopy of the background quasars. One might therefore hope to find Lyman-α emission from these objects superimposed on the Lyman-α forest of high-redshift quasars. For instance, a recent 30h exposure of the $z = 7$ quasar J1120+0641 utilised a 0.9" slit, and possesses sufficient wavelength coverage to encompass both Mg II absorption and Lyman-α emission at $z > 6.0$ (Bosman et al. 2017). We find no peaks of Lyman-α transmission near the redshifts of Mg II absorbers in that object, even taking into account a possibly large kinematic offset ($\pm$2000 km s^{-1}) between the transitions. Assuming a Lyman-α emission line width of ~ 200 km s^{-1} as has been found in typical high-redshift Lyman-α emitters, we are able to put a conservative constraint on the line flux of the absorbing galaxy of $F_{{\rm Ly}\alpha} < 9 \cdot 10^{-19}$ erg cm^2 s^{-1} if it is indeed located in the same slit as the background quasar. This limit is challenging even with deep exposures of state-of-the-art IFUs; for instance, only five Lyman-α lines fainter than this limit were found in a 27h deep-field exposure with MUSE under good conditions (Bacon et al. 2015).

3.2 $R_{\rm min}$

An intriguing implication of our analytic model is the existence of a *minimum scale of enrichment*, $R_{\rm min} = R(L_{\rm min})$. Equation (8) has the property of making $R_{\rm min}$ only weakly dependant on the choice of β, as shown in Figure 3. This measurement is particularly well-constrained at $z = 5$. For instance, for $M_{\rm min} = -15$ the radius of the smallest enriched region is constrained to be $20 < R_{\rm min} < 40$ ckpc; only enriched regions larger than $R_{\rm min}$ contribute to the observed Mg II budget. These scales are already well resolved by cosmological numerical simulations such as Sherwood or Illustris, as presented in e.g. Keating et al. (2016). It is therefore possible that the disagreements between these simulations and the observed abundance rates of metals are not due to lack of resolution, but rather inadequate prescriptions for metal production and dispersal.

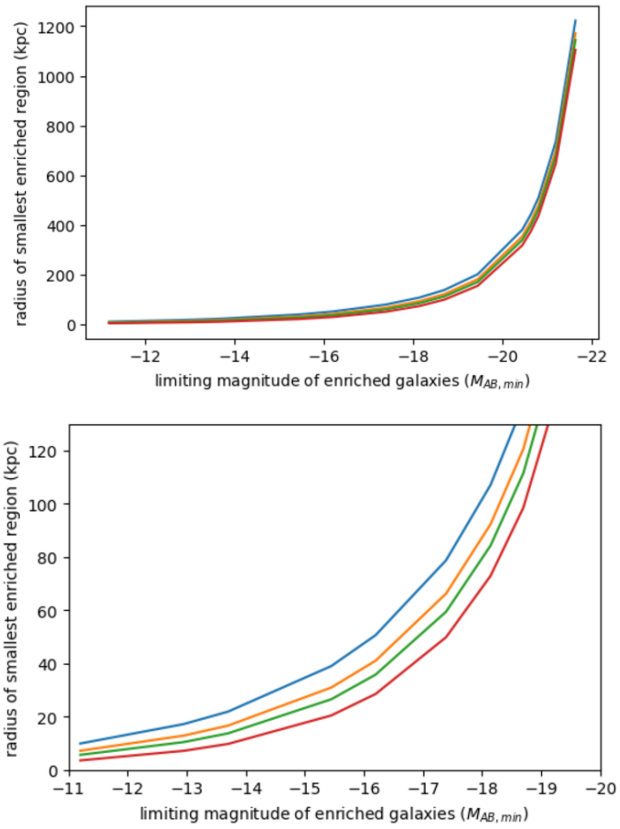

Figure 3. Sizes of the smallest enriched haloes: colours blue to red show $\beta = 0.1, 0.23, 0.3, 0.4$. Bottom is a zoom on the top panel.

The physical meaning of $R_{\rm min}$ constitutes an interesting avenue for future research. If a minimal scale of metal enrichment truly exists, it is likely to be related to single-generation enrichment of the CGM by Pop III stars. However, it is crucial to note that the analysis presented in this paper is concerned only with Mg II absorbers currently accessible to observations, i.e., those with equivalent widths $W_{\rm r} > 0.1$Å. Enrichment weaker than this threshold, if it is present, will be revealed by upcoming next-generation instruments such as ELT HIRES (Marconi et al. 2016). A detailed analysis of the physical meaning of this minimal scale should therefore be reserved until the minimal threshold for enrichment has been established beyond observational limitations.

3.3 Redshift evolution

Beyond $z = 6$, both the occurrence rate of absorbers (dN/dX) and the luminosity function of galaxies (Φ^*, α) become more uncertain by an order of magnitude compared to $z = 5$. The range of possible $R(L)$ distributions therefore increases significantly, as can be seen in Figure 2. Interestingly,

models with large galaxy-absorber separations still require those galaxies to have brightnesses $M_{AB} \gtrsim -15$ for separations $\gtrsim 1.5$". This reflects the fact that the number of bright galaxies at $z \sim 6.5$ is sufficient to explain the number density of absorbers; if the Mg II haloes of those bright galaxies are larger than ~ 100 ckpc, the number of absorbers is exceeded even for the most conservative choices of parameters.

Figure 3 suggests that Mg II haloes were on average smaller at $z \sim 6.5$ compared to $z = 5$, and that faint galaxies make up a larger fraction of absorbers at earlier times. This is consistent with a picture of ongoing star formation and hierarchical mergers. Note, however, that out of the three redshift-dependent observables $\{\Phi^*, \alpha, dN/dX\}$, only one is evolving between $z = 5$ and $z = 6.5$ at more than 1σ significance (see Tables 1 and 3). The difference between $R(L)$ at $z = 5$ and $z \sim 6.5$ is therefore likely driven mostly by a larger range of observationally permitted models, rather than intrinsic evolution.

REFERENCES

Atek, H., Richard, J., Kneib, J.-P., et al. 2015, ApJ, 800, 18

Bacon, R., Brinchmann, J., Richard, J., et al. 2015, A&A, 575, A75

Bergeron, J., & Boissé, P. 1991, A&A, 243, 344

Bosman, S. E. I., Becker, G. D., Haehnelt, M. G., et al. 2017, MNRAS, 470, 1919

Bouwens, R. J., Oesch, P. A., Illingworth, G. D., Ellis, R. S., & Stefanon, M. 2016, ArXiv e-prints, arXiv:1610.00283

Bouwens, R. J., Illingworth, G. D., Oesch, P. A., et al. 2015, ApJ, 803, 34

Chen, H.-W., Wild, V., Tinker, J. L., et al. 2010, ApJ, 724, L176

Chen, S.-F. S., Simcoe, R. A., Torrey, P., et al. 2016, ArXiv e-prints, arXiv:1612.02829

Churchill, C. W., Nielsen, N. M., Kacprzak, G., & Trujillo, S. 2013, in American Astronomical Society Meeting Abstracts, Vol. 221, American Astronomical Society Meeting Abstracts #221, 227.04

Churchill, C. W., Rigby, J. R., Charlton, J. C., & Vogt, S. S. 1999, ApJS, 120, 51

Codoreanu, A., Ryan-Weber, E. V., Crighton, N. H. M., et al. 2017, ArXiv e-prints, arXiv:1708.00304

Finkelstein, S. L., Ryan, Jr., R. E., Papovich, C., et al. 2015, ApJ, 810, 71

Forero-Romero, J. E., Yepes, G., Gottlöber, S., & Prada, F. 2012, MNRAS, 419, 952

Gauthier, J.-R. 2013, MNRAS, 432, 1444

Ishigaki, M., Kawamata, R., Ouchi, M., et al. 2015, ApJ, 799, 12

Kacprzak, G. G., Churchill, C. W., Barton, E. J., & Cooke, J. 2011, ApJ, 733, 105

Keating, L. C., Puchwein, E., Haehnelt, M. G., Bird, S., & Bolton, J. S. 2016, MNRAS, 461, 606

Livermore, R. C., Finkelstein, S. L., & Lotz, J. M. 2017, ApJ, 835, 113

Marconi, A., Di Marcantonio, P., D'Odorico, V., et al. 2016, in Proc. SPIE, Vol. 9908, Ground-based and Airborne Instrumentation for Astronomy VI, 990823

Mason, C. A., Trenti, M., & Treu, T. 2015, ApJ, 813, 21

Matejek, M. S., & Simcoe, R. A. 2012, ApJ, 761, 112

Ménard, B., & Chelouche, D. 2009, MNRAS, 393, 808

Nielsen, N. M., Churchill, C. W., & Kacprzak, G. G. 2013, ApJ, 776, 115

Stark, D. P., Ellis, R. S., Chiu, K., Ouchi, M., & Bunker, A. 2010, MNRAS, 408, 1628

Steidel, C. C. 1995, in QSO Absorption Lines, ed. G. Meylan, 139

Steidel, C. C., Dickinson, M., & Persson, S. E. 1994, ApJ, 437, L75

Weiner, B. J., Coil, A. L., Prochaska, J. X., et al. 2009, ApJ, 692, 187